Astron. Astrophys. 71, 275—282 (1979)

ASTRONOMY AND ASTROPHYSICS

Ammonia in Orion

T. L. Wilson, D. Downes, and J. Bieging

Max-Planck-Institut für Radioastronomie, Auf dem Hügel 69, D-5300 Bonn 1, Federal Republic of Germany

Received April 10, 1978

Summary. New observations separate the ammonia line emission in Orion into two spatial components, a background ridge and an unresolved core. The background is probably the same ridge seen in CO and other molecules. The unresolved core is centered on the infrared cluster in the Kleinmann-Low nebula. In the metastable lines of NH_3, the core source has three velocity components: (i) a strong, narrow feature at $V_{LSR}=9$ km s^{-1}, which is optically thick (from the ratio of the hyperfine components) and has a rotational temperature $T_{1,1}^{2,2}\sim 60$ K; (ii) a weaker, narrow feature at $V_{LSR}=3$ km s^{-1}, which appears to be optically thin and to come from a hot region ($T_{rot}>200$ K); (iii) a broad line, with a width ~ 50 km s^{-1} and a rotational temperature of ~ 40 K. Three independent methods of analysis show that the 9 km s^{-1} narrow-line component is emitted in a region $\leqq 20''$ in size, in agreement with the results of Barrett et al. (1977). The broad component is spatially unresolved, and is probably the high-velocity outflow seen in other molecular lines. We obtain a lower limit of 350, for the $^{14}NH_3/^{15}NH_3$ ratio, close to the terrestrial value.

Key words: interstellar molecules — Orion nebula

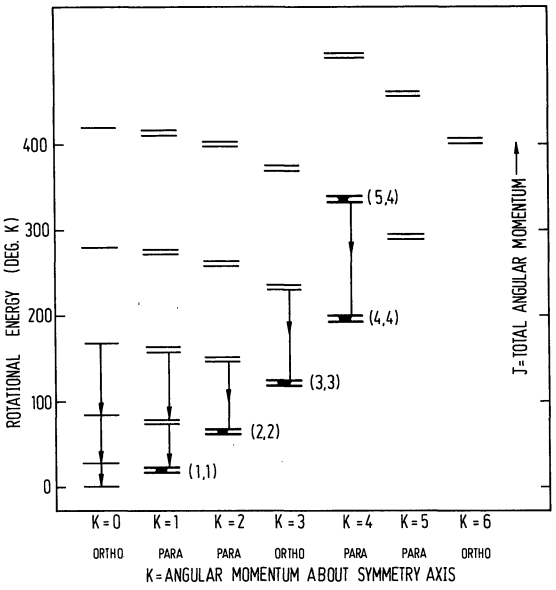

Fig. 1. Energy level diagram for NH_3 in its ground vibrational state. Doublet splittings are expanded by a factor of 10. The transitions observed in this paper are marked with heavy shading and are indicated with their rotational quantum numbers (J,K). The arrows indicate allowed transitions for the lower-lying levels (after Rank et al., 1971)

Ammonia has many spectral lines at frequencies 22–25 GHz which become excited under widely differing physical conditions. The molecule is thus a useful probe of molecular clouds, especially since these lines can all be observed with the same angular resolution. This paper presents new measurements of the NH_3 transitions marked by thick shading in the energy-level diagram in Fig. 1. The radiative half-life for the lines from metastable levels, where $J=K$, is $\gtrsim 10^6$ s, whereas the time for radiative decay from non-metastable levels ($J\neq K$) to the corresponding metastable level is less than 10^2 s (as long as optical depths in the infrared lines of NH_3 are small).

Send offprint requests to: D. Downes

Barrett et al. (1977) measured metastable lines in Orion with an angular resolution of 1'.4, and argued that the main NH_3 emission came from a region $\sim 10''$ in size. We have mapped the (1,1), (2,2), and (3,3) lines in the region contained in the beam of Barrett et al. and confirm their results. We have also detected the high-velocity outflow in the Kleinmann-Low nebula, and have obtained a lower limit on the ratio of $^{14}NH_3$ to $^{15}NH_3$.

Observations

The data were taken in October 1976 with the Effelsberg 100-m telescope. At 23 GHz, the half-power beamwidth is $40''\times 43''$ (az. × el.), and in the zenith, the beam and aperture efficiencies are respectively 0.37 ± 0.05 and

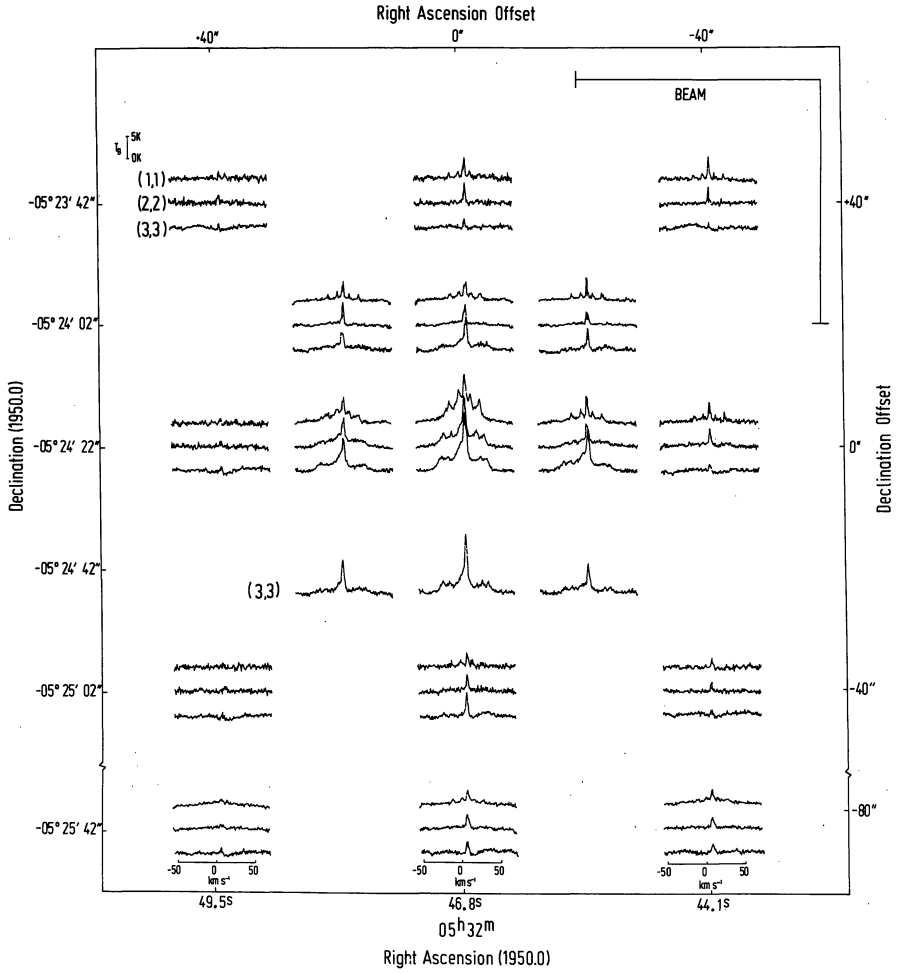

Fig. 2. Spectra of the (1,1), (2,2), and (3,3) transitions of NH_3, plotted in R.A. and Dec

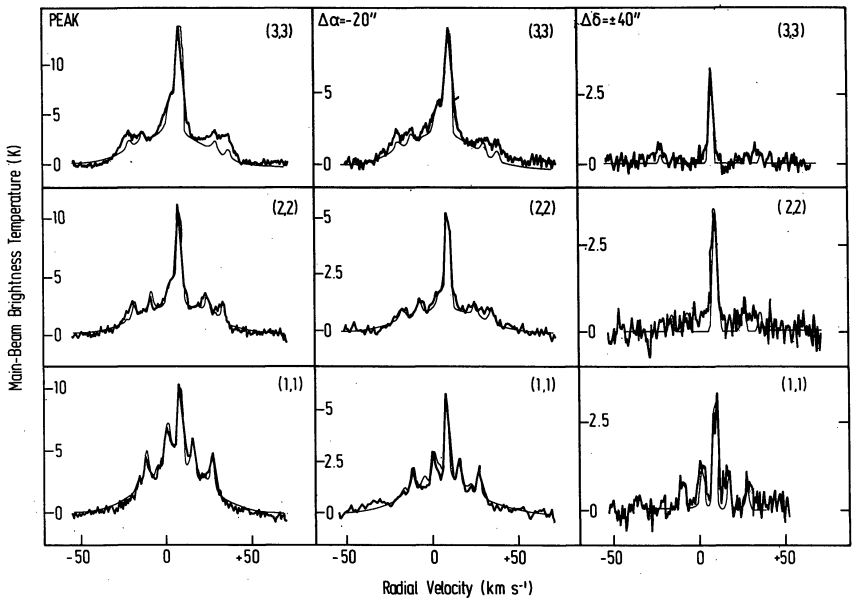

Fig. 3. Spectra of metastable ammonia lines at representative positions in Orion. The heavy lines are the observations, the light curves are the gaussian fits. Offsets are relative to $05^h32^m46^s.8$, $-05°24'22"$ (1950.0)

Table 1. NH_3 line parameters

NH_3 Feature	Transition (J, K)	Main Beam Line T_b (deg. K)	Full Width to Half-Power (km s^{-1})	LSR Radial Velocity (km s^{-1})	Optical Depth τ	Column Density (10^{13} cm^{-2})
Core Region						
Narrow Feature at 9 km s^{-1}	(1,1)	6.7	3.0	8.0	2.0	1180[a]
	(2,2)	8.0	3.0	7.7	3.5	970[a]
	(3,3)	10.0	3.2	7.3	3.0	700[a]
	(4,4)	4.2	∿3.5	8.6	-	15
	(5,4)	0.8	∿3	7.2	-	3
Narrow Feature at ∿3 km s^{-1}	(1,1)	~1.8	3.0	3.0	-	15
	(2,2)	1.9	3.0	2.2	-	8
	(3,3)	4.2	4.5	2.3	-	20
	(4,4)	2.5	∿3.5	3.3	-	8
	(5,4)	0.7	∿3	3.3	-	3
Broad Feature	(1,1)	3.4	46	5.5	-	220
	(2,2)	2.6	50	∿0	-	140
	(3,3)	3.9	55	∿3	-	200
Total in all levels we have observed						3482
Molecular Ridge at = δ ±40" from Core						
Narrow Feature at ∿9 km s^{-1}	(1,1)	3.1	2.7	10.0[b] 7.9	∿1.1	590[a]
	(2,2)	3.5	2.8	10.0 8.3	∿1.5	390[a]
	(3,3)	3.5	2.5	8.8 7.0	-	8
Total						988

[a] Assumed $T_{ex}=70$ K

[b] Upper and lower values are for $\delta=+40''$ and $-40''$ respectively

0.29 ± 0.04, for the inner 80-m of the dish. The main-beam brightness temperature scale is probably accurate to 20%. The receiver was a parametric amplifier followed by a 384-channel autocorrelation spectrometer, and the system temperature was ~200 K in the zenith. The spectrometer was split so that the (1,1) and (2,2) lines could be measured simultaneously, with a resolution of 63 kHz (0.8 km s^{-1}). The (3,3) and (4,4) transitions were observed separately, with a resolution of 31.5 kHz (0.4 km s^{-1}). Off-source reference scans were taken 7^m west of the KL nebula.

Figure 2 shows the (1,1), (2,2), and (3,3) spectra on (α, δ) axes. For the outer positions in Fig. 2, line parameters could be measured directly from the spectra. For the more complex profiles near the map center, we fitted two velocity features with distinct hyperfine satellite components, and one broad component. Because the full width to half-power of the broad component is >20 km s^{-1}, the individual hyperfine components are blended, and we approximated the line shape by a single gaussian. For the narrow lines, the free parameters in the fits were linewidth, peak temperature, optical depth and LSR radial velocity, while relative hyperfine intensities and relative velocities were fixed (Kukolich, 1967). Figure 3 shows typical examples of fitted profiles.

As a check on our results, we also smoothed our data with a gaussian weighting function to the angular resolution of 1'.4 used by Barrett et al. (1977), and converted their data to a scale of main-beam T_b. Our convolved spectra are in excellent agreement with the (1,1), (2,2), and (3,3) profiles from Barrett et al.

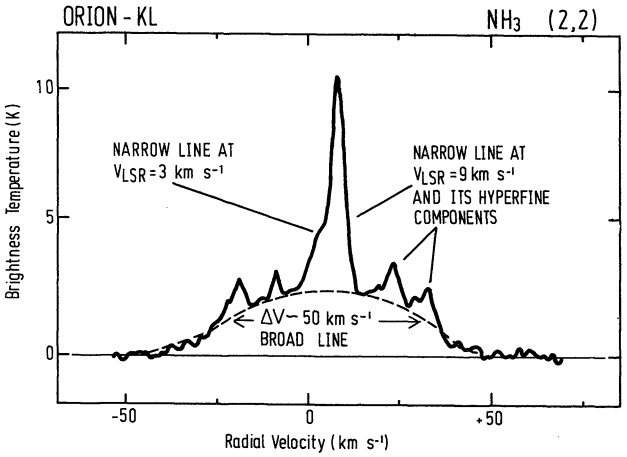

Fig. 4. Spectrum of the (2,2) transition of ammonia at the position of peak signal in the KL nebula, with the decomposition into narrow and broad lines described in the text

Spectra of the Metastable Lines

Our data taken toward the Kleinmann-Low nebula show three features (Fig. 4):

(1) a strong ($T_b\sim6$–10 K), narrow ($\Delta V\sim3$–4 km s^{-1}) feature at $V_{LSR}\sim9$ km s^{-1}.

(2) a weaker ($T_b\sim0.5$–2 K), narrow ($\Delta V\sim3$–6 km s^{-1}) feature at $V_{LSR}\sim3$ km s^{-1};

(3) a broad ($\Delta V\sim50$ km s^{-1}) line, also centered at $V_{LSR}\sim9$ km s^{-1}.

Table 1 summarizes the parameters of these features at on- and off-source positions. In order to derive the optical depths in Table 1, we assumed that the main and satellite groups of hyperfine components have the same excitation temperature. At 24 GHz, the column density in the lower of the two levels of a transition is related to the integrated optical depth by

$$N'_{J=K,K}=3.4\ 10^{12}\ (J+1)J^{-1}\int\tau T_{ex}dV \qquad (1)$$

where the integral is taken over all hyperfine components. T_{ex} is the excitation temperature for the given transition, N is in cm^{-2}, and V is in km s^{-1}. Eq. (1) was derived with the assumption that T_{ex} is much larger than the separations of the NH_3 levels. The column densities in Table 1 are the sums of the upper and lower levels of the listed transitions, calculated from

$$N_{J=K,K}=N'_{J,K}[1+\exp(-1.1/T_{ex})]. \qquad (2)$$

We assumed in Table 1 that $T_{ex}=70$ K. At positions where we had only an upper limit to the optical depth, we took $\tau T_{ex}=T_b$, the main-beam brightness temperature. We varied the parameters of the velocity components in the fits, and we estimate that the un-

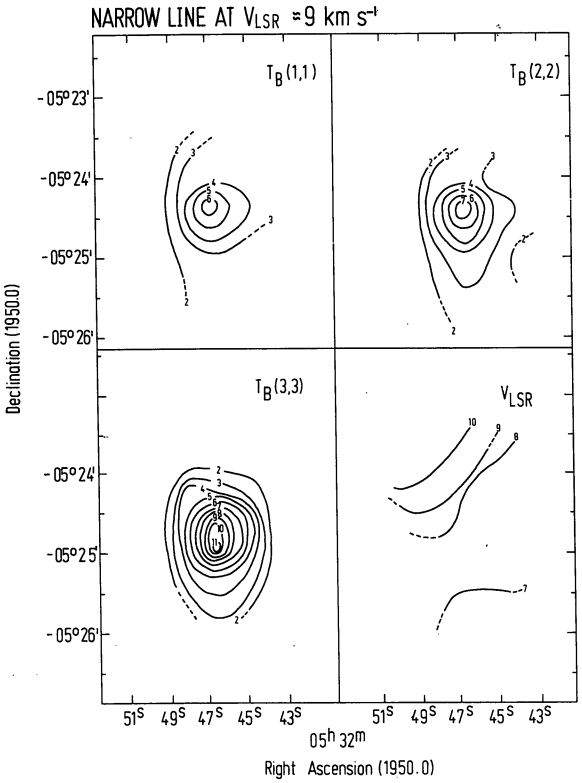

Fig. 5. Maps of line brightness temperature in the (1,1), (2,2), and (3,3) transitions of NH_3 for the narrow line at 9 km s^{-1}. Contour units are deg. K. The map at lower right shows the LSR radial velocity in these three transitions as a function of position (contour labels are km s^{-1})

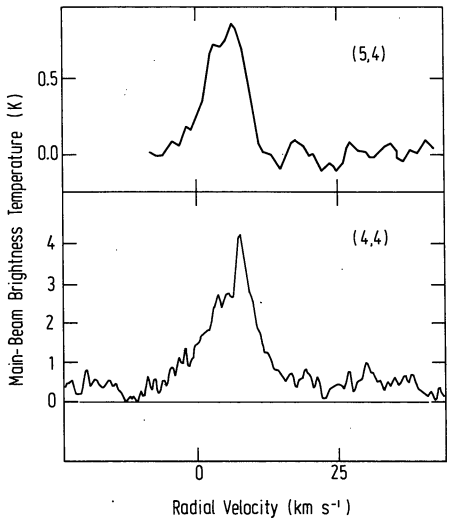

Fig. 6. Spectra of the (4,4) and (5,4) transitions of NH_3 at the core of the KL nebula. A comparison of this Figure with Fig. 3 shows the increasing contribution of the feature at 3 km s^{-1} at higher energy levels

certainties in the column densities are ~20%. The column densities for the broad line are especially sensitive to small deviations from the assumed gaussian line shape.

1. The Narrow Feature at $V_{LSR} = 9$ km s^{-1}

The distribution of the 9 km s^{-1} narrow feature is given in Fig. 5. The maps show that two spatial components are present: (a) an extended background (size >1'.5 in Dec.), which is presumably the central "ridge" of the Orion Molecular Cloud seen in other molecular lines; (b) a strongly peaked core region, centered on

R.A. = $05^h32^m46^s.8 \pm 0^s.2$

Dec. = $-05°24'26'' \pm 6''$ (1950.0).

a) The Background Ridge

Figure 5 (lower right) shows the distribution of radial velocities in the background ridge, derived from the average velocities of the (1,1), (2,2), and (3,3) transitions. The trend agrees with that observed in other molecules, with an increase in velocity from the southwest to the northeast corners of the map. From CO measurements, Liszt et al. (1974) suggested that the core of the Orion molecular cloud was rotating about an east-west axis. Our velocity data are not consistent with such a rotation. Ho and Barrett (1977) resolve the 9 km s^{-1} feature in the (2,2) line into two further components at 7.6 and 9.6 km s^{-1}. They suggest that the apparent velocity gradient in the ridge can be explained simply by the superposition of two separate clouds.

b) The Core Source

We can estimate the size of the core source by three independent methods.

(a) From the column densities at the peak and 20" from the peak, the size is $\leqq 20''$. The largest uncertainty is in the separation of the NH_3 spectrum into different velocity components, but all of these components are point sources in our beam. Although the brightness temperature distribution of the NH_3 appears to be slightly extended in Fig. 5, one must remember (i) to subtract the contribution of the background ridge, and (ii) that because the NH_3 is optically thick, the source size obtained from the brightness temperature will be an overestimate of the "true" size obtained from the column density.

(b) If the NH_3 is thermalized, that is, its excitation temperature, T_{ex}, equals the kinetic temperature, then the beam filling factor, f, is given by

$$T_L = f(T_{ex} - 2.7)(1 - e^{-\tau}). \quad (3)$$

We take the kinetic temperature to be $\geqq 70$ K, the brightness temperature of ^{12}CO measured with a 1' beam (Liszt et al., 1974). From the values of τ and T_L given in Table 1, we derive $f \leqq 0.17$, which corresponds to a size of $\leqq 18''$ for the NH_3 core.

(c) We can also take the ratio of our main-beam brightness temperatures for the (1,1), (2,2), and (3,3) lines to those measured by Barrett et al. with a 1'.4 beam. The average ratio is 4.4, with a scatter of 0.6. Within the errors, this ratio is consistent with a point source.

These three methods therefore yield a size of $\leqq 20''$ for the NH_3 core. This angle corresponds to $\leqq 0.05$ pc at a distance of 500 pc, and is consistent with the core size derived by Barrett et al. (1977).

2. *The Narrow Feature at $V_{LSR} \sim 3$ km s^{-1}*

The weaker narrow feature, at a velocity of 3 km s^{-1}, also seen by Barrett et al. (1977) is heavily blended with the 9 km s^{-1} feature (cf. Fig. 4), and its parameters are somewhat uncertain. The fits to the data on the peak and 20″ from the peak are consistent with a spatially unresolved source, located at the same position as the core region at 9 km s^{-1}. The 3 km s^{-1} feature is especially prominent in the (4,4), and (5,4) spectra in Fig. 6. The rapid increase of the line brightness temperature with the rotational quantum number J, implies an optically thin, hot gas. A number of other molecules have also been detected in Orion at ~3–5 km s^{-1}, including, most recently, ethyl cyanide (Johnson et al., 1977).

3. *The Broad Line*

The component with a line width of 50 km s^{-1} has now been seen in many molecules, most prominently in the $J=1\rightarrow 0$, $2\rightarrow 1$, and $3\rightarrow 2$ transitions of CO (Zuckerman et al., 1976; Kwan and Scoville, 1976; Wannier and Phillips, 1977; Phillips et al., 1977). Our data show that this feature is spatially unresolved (size $\leqq 20''$), and centered on the core region, that is, the position of the infrared cluster in the KL nebula. The line shape in the ammonia (1,1, and (2,2) transitions is gaussian. The fit is somewhat worse for the (3,3) transition (Fig. 3), and might imply a change of line shape with increasing quantum number.

If the high-velocity NH_3 is optically thin, the ratio of NH_3 column density in the high-velocity gas to that in the narrow feature at 9 km s^{-1} is 0.2 for the (1,1) line, 0.1 for the (2,2) line and 0.3 for the (3,3) line. These values are based on an assumed excitation temperature of 70 K for the optically thick narrow-line NH_3 at 9 km s^{-1}. Since the high-velocity NH_3 may be in a smaller region than the quiescent gas at 9 km s^{-1}, the volume density of the NH_3 may be higher for the broad-line gas than for the narrow-line gas.

Rotational Temperatures

Table 2 lists NH_3 rotational temperatures derived from the ratio of column densities for given levels. We assumed that the relevant lines were emitted in the same volume with the same excitation temperatures. Only the results at the position of the unresolved core source were accurate enough to give rotational temperatures, which we list for combinations of para levels only. The time for an interchange between ortho and para populations might be $\sim 10^9$ yr, under interstellar conditions (Cheung et al., 1969). Because of the decoupling of the ortho and para NH_3, their populations might not be related by the usual statistical weights (see discussion below).

Table 2. NH_3 rotational temperatures in the Orion core source

NH_3 levels involved		Rotational temperatures		
		Narrow feature at 9 km s^{-1}	Narrow feature at 3 km s^{-1}	Broad feature
(1,1)	(2,2)	60±20 K	—	40±20 K
(1,1)	(4,4)[a]	~30 K	—	—
(2,2)	(4,4)[a]	30±10 K	>200 K	—
(4,4)[a]	(5,4)[a]	85 K	~100 K	—

[a] NH_3 emission assumed to be optically thin

1. For the Narrow Feature at 9 km s^{-1}, the rotational temperature $T_{1,1}^{2,2}=60\pm 20$ K is consistent with our estimates of excitation and kinetic temperatures, made on the basis of the high optical depth. It is thus a further indication that the estimate of the angular size of the NH_3 line-emitting region is correct. The rotational temperature obtained from the (1,1) and (4,4) data is about one half of that obtained from the (1,1), and (2,2) results. We assumed that the (4,4) line was optically thin, so the rotational temperature might be underestimated. If instead, the optical depth of the (4,4) line were ~0.5, $T_{1,1}^{4,4}$ would agree with $T_{1,1}^{2,2}$.

A model based on excitation via the Far Infrared continuum has been calculated by Sweitzer (1977). This model fits our results for the 9 km s^{-1} data very well, and requires an H_2 density of 10^6 cm^{-3}.

2. For the Narrow Feature at 3 km s^{-1}, the column density in the (1,1) line is very uncertain. The ratio of the column densities in the (2,2) and (4,4) lines confirm that the rotational temperature of the NH_3 at 3 km s^{-1} is considerably larger than that of the 9 km s^{-1} feature. The rotational temperature $T_{4,4}^{5,4}$ in the 3 km s^{-1} feature is ~100 K. For collisional excitation alone the strong (5,4) emission would require a particle density $>10^8$ cm^{-3}.

3. For the Broad Feature, the rotational temperature $T_{1,1}^{2,2}=40\pm 20$ K seems inconsistent with the kinetic temperature $\geqq 100$ K estimated for the high velocity CO (Phillips et al., 1977). However, the NH_3 rotational temperature was obtained by assuming that the (1,1), and (2,2) lines are optically thin and in LTE. This discrepancy between NH_3 and CO may thus be an indication of non-equilibrium populations in the NH_3

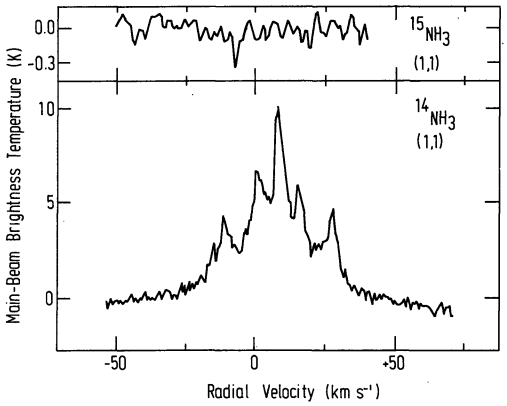

Fig. 7. (upper) Search for the (1,1) transition of $^{15}NH_3$; (lower) comparison spectrum of the (1,1) transition of $^{14}NH_3$. Both spectra were taken at the position of peak signal in the KL nebula

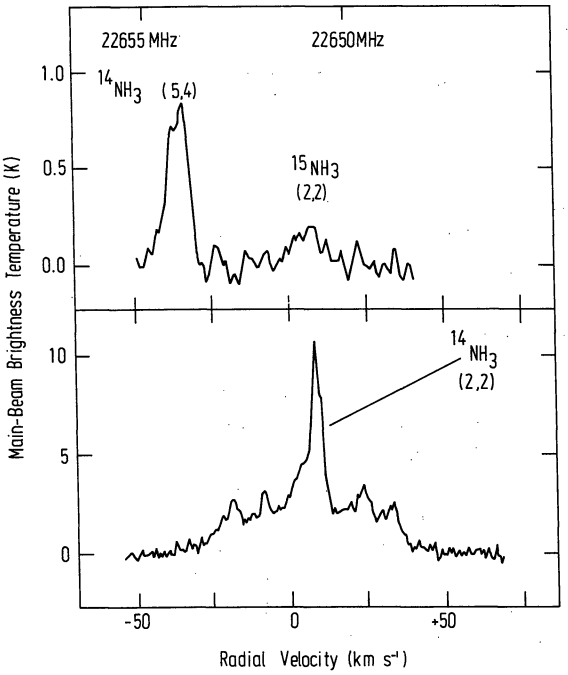

Fig. 8. (upper) Possible detection of the (2,2) transition of $^{15}NH_3$; (lower) comparison spectrum of the (2,2) transition of $^{14}NH_3$. Both spectra were taken at the position of peak signal in the KL nebula

in the high-velocity flow, or else that the NH_3 and CO are not in exactly the same regions.

Search for the $^{15}NH_3$ Isotope

Figures 7 and 8 show the results of our search for $^{15}NH_3$. Although a weak signal appears at the correct velocity in the (2,2) line, we can only give an upper limit for the (1,1) line. To estimate the $^{14}NH_3/^{15}NH_3$ ratio, we made the following assumptions:

a) the $^{14}NH_3/^{15}NH_3$ ratio in the unobserved levels is the same as the ratio in the (1,1) and (2,2) levels;

Table 3. Limits on the ratio of $^{14}NH_3$ to $^{15}NH_3$

Transition:	(1,1)	(2,2)
Column density:		
$^{14}NH_3$	$1.4\ 10^{16}$ cm^{-2}	$1.1\ 10^{16}$ cm^{-2}
$^{15}NH_3$	$\leqq 0.8\ 10^{13}$ cm^{-2}	$\leqq 3.1\ 10^{13}$ cm^{-2}
Limit on ratio:		
$^{14}NH_3/^{15}NH_3$	$\geqq 1800$	$\geqq 350$

b) the excitation temperature of the (1,1), and (2,2) lines is 70 K;

c) the $^{15}NH_3$ is optically thin;

d) the $^{14}NH_3$ and $^{15}NH_3$ occupy the same volume and have the same linewidths.

Table 3 is a comparison of the column densities of the (1,1), and (2,2) lines. The ratio of $^{14}NH_3$ to $^{15}NH_3$ from the (1,1) transition is $\geqq 1800$, while that from the (2,2) transition is $\geqq 350$, not far from the terrestrial value of 279. Because of the poor sensitivity, the $^{14}NH_3/^{15}NH_3$ ratio from the (2,2) levels should be taken as the more conservative lower limit.

Relation of Ortho- to Para-NH_3

Cheung et al. (1969) recognized that the column densities in the ortho and para ladders in interstellar NH_3 are not related by the statistical weights of the levels. The relation is further complicated by the differing spatial distributions of the ortho and para lines observed in some sources. For example, our map of the NH_3 emission toward W3 (OH) (Wilson et al., 1978) showed that the spatial extent of the (3,3) line was about half that of the (1,1), and (2,2) lines. Since our maps do not resolve the core region in Orion, we cannot be sure of the relative sizes of the (1,1), (2,2), and (3,3) emitting regions.

At the position of the core source, the column density of the (3,3) level in the 9 km s^{-1} narrow feature is 0.6 of the value expected if the (1,1), (2,2), and (3,3) levels were in LTE with the same excitation temperatures. Considering the uncertainties in the rotational temperature $T_{1,1}^{2,2}$, the column density in the (3,3) level is consistent with those in the (1,1), and (2,2) levels.

For the 3 km s^{-1} feature, the comparison of ortho and para lines is even more uncertain, but here the population in the (3,3) level is also roughly consistent with those in the (1,1), and (2,2) levels.

The column density in the broad line in the (3,3) level is twice the LTE value expected from the (1,1), and (2,2) results. However, this difference in the ortho-to-para ratio lies within the errors assigned to the rotational temperature $T_{1,1}^{2,2}$ for the broad line, so these results are also consistent with LTE, with large errors.

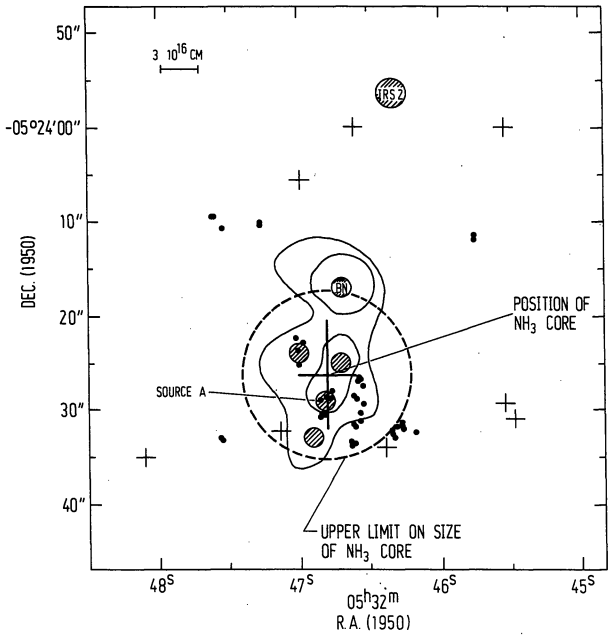

Fig. 9. The large cross indicates the positional uncertainty of the unresolved NH_3 core source. The dashed circle gives the upper limit for the sizes of both the NH_3 narrow-line core source and the NH_3 broad line. The ammonia data are superimposed on the composite diagram from Genzel et al. (1978), which show infrared contours at 20 μ (Rieke et al., 1973), infrared point source (shaded circles, Rieke et al., Wynn-Williams and Becklin, 1974), low velocity H_2O masers (black dots, Genzel et al., 1978), and high velocity H_2O masers (small crosses, Genzel and Downes, 1977). Source A is the dominant OH, H_2O, and SiO source, with a velocity range of at least 22 km s^{-1}

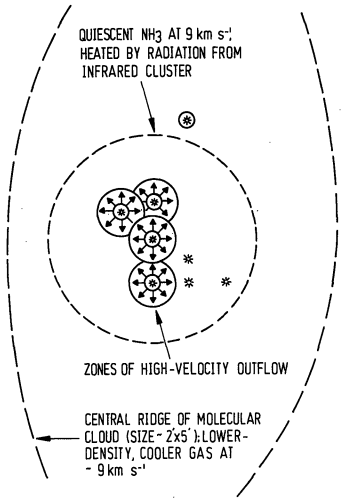

Fig. 10. A possible interpretation of the ammonia observations. The broad-line NH_3 comes from expanding envelopes around the stars in the KL infrared cluster. The ambient NH_3 external to these envelopes is heated by the radiation from the cluster and constitutes the NH_3 core region in the narrow line at 9 km s^{-1}. The core region is in turn imbedded in the lower-density "ridge" of the Orion Molecular Cloud

Comparison with Other Maps

The small core region which we observe in NH_3 is not at all visible on the maps of ^{13}CO (Liszt et al., 1974), H_2CO at 2 mm (Kutner et al., 1971, 1976), or N_2H^+, HCO^+ and CN (Turner and Thaddeus, 1977). The $J=1\rightarrow0$ line of ^{13}CO and the 2-mm lines of H_2CO presumably become optically thick at lower densities than does NH_3, and delineate mainly the central part of the $2' \times 5'$ ridge of the molecular cloud, rather than the unresolved core which dominates the NH_3 maps.

There is evidence for the core on the maps of HCN (Turner and Thaddeus, 1977), H_2CO at 2 cm (Evans et al., 1975), and on the continuum maps at 1 mm, 100 μ and 33 μ (Westbrook et al., 1976; Harvey et al., 1974; Werner et al., 1976; Beichman et al., 1978). Even on most of these maps, however, the half-power extent is considerably larger than on our NH_3 map. In NH_3, there is a decrease in both the brightness temperature and in the optical depth, away from the core source. Hence the difference in the distribution of NH_3 and H_2CO at 2 cm, for example, is a true difference in the column densities of these molecules, rather than an excitation effect.

The most detailed observations with which the NH_3 data can be compared are the near-infrared maps (Rieke et al., 1973; Wynn-Williams and Becklin, 1974) and the OH, SiO, and H_2O maser-line maps (Hansen et al., 1977; Norris et al., 1978; Moran et al., 1977; Genzel et al., 1978). Figure 9 shows the position and size limit for the NH_3 in both the narrow line at 9 km s^{-1} and in the broad line, superimposed on the contours of 20 μ radiation and the positions of H_2O masers.

The position of the NH_3 core coincides within the errors with the source marked "*A*" on the map. This is the strongest infrared source in KL at wavelengths $\geqq 30\,\mu$. It is designated "core of KL" on the map by Wynn-Williams and Becklin (1974) and "IRc4" on the map by Rieke et al. (1973). It is the dominant OH, H_2O, and SiO source in Orion, with a velocity range in these molecules of at least 22 km s^{-1}, and an angular extent of a few arc s, from VLBI and infrared measurements.

Figure 10 is a possible interpretation of the observations. The stars of the infrared cluster in KL are losing mass, as is indicated by the maser lines, particularly the SiO and the so-called "low-velocity" H_2O lines. A further indication of the mass loss may be the 100 km s^{-1} broad wings of the Brackett α line in the BN object (Hall et al., 1978). The broad feature in NH_3, CO and other molecules probably arises in the extended envelopes of these stars, or in wind-driven shells of the type described by Weaver et al. (1977). The rate of mass loss from the stars, as estimated from the broad wings of the CO lines, is an order of magnitude greater than that observed in Herbig Ae and Be stars (Zuckerman et al., 1976). The extent of the expanding envelopes is probably a few arc s for individual stars. However, the infrared and maser maps indicate that, in addition to the luminous Source A, there are four to ten other stars in the cluster, each of

which may have an envelope which contributes to the "broad feature" observed with 40″ to 60″ beams.

The ambient gas at 9 km s^{-1} in the vicinity of the infrared cluster is heated by the radiation of the cluster, and constitutes the "unresolved core" of the narrow-line NH_3 feature at 9 km s^{-1}. Farther away from the infrared cluster is the lower-density, cooler gas which makes up the central "ridge" of the Orion Molecular Cloud.

References

Barrett, A. H., Ho, P. T. P., Myers, P. C.: 1977, *Astrophys. J.* **211**, L39

Beichman, C. A., Dyck, H. M., Simon, T.: 1978, *Astron. Astrophys.* **62**, 261

Cheung, A. C., Rank, D. M., Townes, C. H., Knowles, S. H., Sullivan, W. T.: 1969, *Astrophys. J.* **157**, L13

Evans, N. J., Zuckerman, B., Sato, T., Morris, G.: 1975, *Astrophys. J.* **199**, 383

Genzel, R., Downes, D.: 1977, *Astron. Astrophys.* **61**, 117

Genzel, R., Downes, D., Moran, J. M., Johnston, K. J., Spencer, J. H., Walker, R. C., Haschick, A., Matveyenko, L. I., Kogan, L. R., Kostenko, V. I., Rönnäng, B., Rydbeck, O. E. H., Moiseev, I. G.: 1978, *Astron. Astrophys.* **66**, 13

Hall, D. N. B., Kleinmann, S. G., Ridgway, S. T., Gillett, F. C.: 1978, *Astrophys. J.* (in press)

Hansen, S. S., Moran, J. M., Reid, M. J., Johnston, K. J., Spencer, J. H., Walker, R. C.: 1977, *Astrophys. J.* **218**, L65

Harvey, P. M., Gatley, I., Werner, M. W., Elias, J. H., Evans, N. J., Zuckerman, B., Morris, G., Sato, T., Litvak, M. M.: 1974, *Astrophys. J.* **189**, L87

Ho, P. T. P., Barrett, A. H.: 1977, *Bull. Am. Astron. Soc.* **9**, 575

Johnson, D. R., Lovas, F. J., Gottlieb, C. A., Gottlieb, E. W., Litvak, M. M., Guelin, M., Thaddeus, P.: 1977, *Astrophys. J.* **218**, 370

Kukolich, S. G.: 1967, *Phys. Rev.* **156**, 83

Kutner, M., Thaddeus, P., Jefferts, K. B., Penzias, A. A., Wilson, R. W.: 1971, *Astrophys. J.* **164**, L49

Kutner, M. L., Evans, N. J., Tucker, K. D.: 1976, *Astrophys. J.* **209**, 452

Kwan, J., Scoville, N.: 1976, *Astrophys. J.* **210**, L39

Liszt, H. S., Wilson, R. W., Penzias, A. A., Jefferts, K. B., Wannier, P. G., Solomon, P. M.: 1974, *Astrophys. J.* **190**, 557

Moran, J. M., Johnston, K. J., Spencer, J. H., Schwartz, P. R.: 1977, *Astrophys. J.* **217**, 434

Norris, R. P., Booth, R. S., McLaughlin, W.: 1978 (in preparation)

Phillips, T. G., Huggins, P. J., Neugebauer, G., Werner, M. W.: 1977, *Astrophys. J.* **217**, L161

Rank, D. M., Townes, C. H., Welch, W. J.: 1971, *Science* **174**, 1083

Rieke, G. H., Low, F. J., Kleinmann, D. E.: 1973, *Astrophys. J.* **186**, L7

Sweitzer, J.: 1977, Ph. D. Thesis, University of Chicago

Turner, B. E., Thaddeus, P.: 1977, *Astrophys. J.* **211**, 755

Wannier, P. G., Phillips, T. G.: 1977, *Astrophys. J.* **215**, 796

Weaver, R., McCray, R., Castor, J., Shapiro, P., Moore, R.: 1977, *Astrophys. J.* **218**, 377

Westbrook, W. E., Werner, M. W., Elias, J. H., Gezari, D. Y., Hauser, M. G., Lo, K. Y., Neugebauer, G.: 1976, *Astrophys. J.* **209**, 94

Werner, M. W., Gatley, I., Harper, D. A., Becklin, E. E., Loewenstein, R. F., Telesco, C. M., Thronson, H. A.: 1976, *Astrophys. J.* **204**, 420

Wilson, T. L., Bieging, J., Downes, D.: 1978, *Astron. Astrophys.* **63**, 1

Wynn-Williams, C. G., Becklin, E. E.: 1974, *Publ. Astron. Soc. Pacific* **86**, 5

Zuckerman, B., Kuiper, T. B. H., Rodriguez Kuiper, E. N.: 1976, *Astrophys. J.* **209**, L137